Some applications of the eikonal model with Coulomb and curvature corrections in pp and $\bar{p}p$ scattering

Phuoc Ha*

Department of Physics, Astronomy and Geosciences, Towson University, Towson, Maryland 21252, USA

(Received 27 December 2022; accepted 21 April 2023; published 15 May 2023)

Using a simple eikonal approach to the treatment of Coulomb-nuclear interference and form-factors effects and taking into account the curvature effects in high-energy pp and $\bar{p}p$ scattering, we determine the basic parameters B, ρ, and $\sigma_{\rm tot}$ from fits to experiment at $W=\sqrt{s}=53$ GeV, 62.3 GeV, 8 TeV, and 13 TeV. We then investigate the differential cross sections in the dip region for pp and $\bar{p}p$ elastic scattering at $W=53$ GeV and 1.96 TeV. We find that the results of the basic parameters calculated using the simple eikonal approach agree well with the values determined in other analyses. We also find that Coulomb effects are significant in the dip region at 53 GeV and 1.96 TeV, and must be taken into account in searches for odderon effects through cross section differences in that energy region.

DOI: 10.1103/PhysRevD.107.094016

I. INTRODUCTION

In a recent paper [1], we presented an analysis of the Coulomb and form-factor effects in pp scattering based on an eikonal model for the spin-averaged pp scattering amplitude. We note that the study of the Coulomb-nuclear interference and its use to extract ρ has a long history [[2–8] and many others] and that the general nucleon-nucleon scattering theory is reviewed in [9,10] and the status leading up to the LHC is reviewed in [11].

Our eikonal approach [12] was based on a realistic model, which fitted the pp and $\bar{p}p$ data from 4.5 GeV to cosmic ray energies, and was consistent with the phase constraints imposed by analyticity [9]. The model allowed us to calculate the Coulomb and form-factor effects in the scattering without significant approximation at any value of q^2 for which it held, extending beyond the first diffraction minimum in the differential cross section.

In that approach, the spin-averaged pp scattering amplitude was given at small q^2 by

$$f(s,q^2)=-\frac{2\eta}{q^2}F^2(q^2)+e^{i\Phi_{\rm tot}(s,q^2)}f_N(s,q^2). \quad (1)$$

The advantage of this form of the amplitude was that the Coulomb term was real, making it clear that the Coulomb-nuclear interference depended only on the real part of the second term, that was, on the real part of $f_N(s,q^2)$ with a (small) admixture of the imaginary part dependent on the phase $\Phi_{\rm tot}(s,q^2)$. The latter was essentially model independent for any eikonal model consistent with the measured pp and $\bar{p}p$ total cross sections, the forward slope parameters $B=-d\log(d\sigma/dq^2)/dq^2$, and the diffractive structure at larger q^2. We found that $\Phi_{\rm tot}(s,q^2)$ was small and easily parametrized in the small-q^2 region and allowed the simple extraction of ρ from the data.

Here, we modify the approach discussed in [1] to isolate the purely nuclear scattering amplitude, with the mixed Coulomb-nuclear effects contained in a small correction term. We use the result to analyze a model used in recent fits to Coulomb-nuclear interference at high energies [13–15] and very high energies [16,17]. Since the Coulomb and form-factor corrections are effectively model independent, we can proceed to a simpler construction used in various experimental analyses in which the purely nuclear part of the differential cross section is approximated as

$$\frac{d\sigma}{dq^2}(s,q^2)\approx Ae^{-Bq^2+Cq^4-Dq^6+\cdots}, \qquad 0\le q^2\ll 1. \quad (2)$$

Here, B is the usual slope parameter and the parameters $C,D\cdots$ which introduce curvature in $d\sigma/dq^2$ are calculated by using our eikonal model fitted to the high energy pp and $\bar{p}p$ data [18,19]. This reduces the number of free parameters by two relative to those used in other analyses of this type [16,17,20].

Using this approach, we evaluate the basic parameters B, ρ, and $\sigma_{\rm tot}$ at $\sqrt{s}=53$ GeV, 62.3 GeV, 8 TeV, and 13 TeV and find that the results of the basic parameters calculated using our simple eikonal approach agree well with the

*pdha@towson.edu

values determined in other analyses. We also study the differential cross sections in the dip region for pp and $\bar{p}p$ elastic scattering at $W = 53$ GeV and 1.96 TeV. We find that Coulomb effects are significant there and must be taken into account in attempts to detect odderon effects from differences in the pp and $\bar{p}p$ cross sections as studied by the D0 and TOTEM Collaborations [21].

II. SIMPLE EIKONAL APPROACH FOR COULOMB-NUCLEAR INTERFERENCE EFFECTS

In the absence of significant spin effects, the spin-averaged differential cross section for pp and $\bar{p}p$ scattering can be written in terms of a single spin-independent amplitude,

$$f(s,q^2) = i\int_0^\infty dbb(1-e^{2i(\delta_c^{\rm tot}(b,s)+\delta_N(b,s))})J_0(qb), \quad (3)$$

Here, $q^2 = -t$ is the square of the invariant momentum transfer, b is the impact parameter, $\delta_c^{\rm tot}(b,s)$ is the full Coulomb phase shift including the effects of the finite charge structure of the proton, $\delta_N(b,s)$ is the nuclear phase shift, and

$$\delta_c^{\rm tot}(b,s) = \delta_c(b,s) + \delta_c^{FF}(b,s), \quad (4)$$

where δ_c gives the phase shift for a pure Coulomb interaction, and δ_c^{FF} accounts for the effects of the form factors at large momentum transfers or short distances.

Equation (3) can be rearranged in the form,

$$f(s,q^2) = f_c(s,q^2) + f_c^{FF}(s,q^2) + f_{N,c}(s,q^2), \quad (5)$$

where

$$f_c(s,q^2) = i\int_0^\infty dbb(1-e^{2i\delta_c(s,b)})J_0(qb) \quad (6)$$

$$f_c^{FF}(s,q^2) = i\int_0^\infty dbbe^{2i\delta_c(b,s)}(1-e^{2i\delta_c^{FF}(b,s)})J_0(qb) \quad (7)$$

$$f_{N,c}(s,q^2) = i\int_0^\infty dbbe^{2i\delta_c(b,s)+2i\delta_c^{FF}(b,s)}(1-e^{2i\delta_N(b,s)})J_0(qb). \quad (8)$$

Here, $f_c(s,q^2)$ is the Coulomb amplitude without form factors, f_c^{FF} accounts for the effects of the form factors on the Coulomb scattering, and $f_{N,c}$ includes the effects of the nuclear scattering as modified by the Coulomb and form factor effects.

The pure nuclear amplitude $f_N(s,q^2)$ is just

$$f_N(s,q^2) = i\int_0^\infty dbb(1-e^{2i\delta_N(b,s)})J_o(qb). \quad (9)$$

We have studied this in detail in an eikonal model fitted to data on $\sigma_{\rm tot}$, B, and ρ for pp and $\bar{p}p$ scattering from 4.5 GeV to cosmic ray energies [12].

Before going further with Eq. (5), for pp scattering, we can divide out the common Coulomb phase $(4p^2/q^2)^{i\eta}$ [or phase $(4p^2/q^2)^{-i\eta}$ for $\bar{p}p$ scattering] from all terms; f_c is then real.

Using the standard proton charge form factor [22],

$$F_Q(q^2) = \frac{\mu^4}{(q^2+\mu^2)^2}, \quad (10)$$

with $\mu^2 = 0.71$ GeV^2, for pp scattering, we find that for the form-factor corrections to the Coulomb amplitude,

$$f_c(s,q^2) + f_c^{FF}(s,q^2) = -\frac{2\eta}{q^2}\left[1-\left(\frac{q^2}{q^2+\mu^2}\right)^{i\eta} + \left(\frac{q^2}{q^2+\mu^2}\right)^{i\eta}\frac{\mu^8}{(q^2+\mu^2)^4}\right], \quad (11)$$

up to negligible real contributions of order η^2. For $\eta/F_Q^2(q^2) \ll 1$,

$$f_c(s,q^2) + f_c^{FF}(s,q^2) = -\frac{2\eta}{q^2}F_Q^2(q^2)e^{i\Phi_{c,FF}}, \quad (12)$$

$$\Phi_{c,FF}(s,q^2) \approx -\eta\left(\frac{(q^2+\mu^2)^4}{\mu^8}-1\right)\ln\frac{q^2}{q^2+\mu^2}. \quad (13)$$

We can separate $f_{N,c}(s,q^2)$, which includes the effects of the nuclear scattering as modified by the Coulomb and form factor effects into two terms,

$$f_{N,c}(s,q^2) = f_{N,c}^{\rm Corr}(s,q^2) + f_N(s,q^2), \quad (14)$$

where $f_N(s,q^2)$ is the pure nuclear amplitude and $f_{N,c}^{\rm Corr}$ isolates the pieces of the full amplitude which involve both Coulomb-plus-form-factor and nuclear terms in a single small term. This is given for pp scattering by

$$f_{N,c}^{\rm Corr}(s,q^2) = i\int_0^\infty dbb\left(\exp\left[2i\eta\gamma + i\eta\ln\left(\frac{q^2b^2}{4}\right) + 2i\eta\sum_{m=0}^{3}\frac{(\mu b)^m}{2^m\Gamma(m+1)}K_m(\mu b)\right]-1\right)\times(1-e^{2i\delta_N(b,s)})J_0(qb). \quad (15)$$

For $\bar{p}p$ scattering, we just change η to $-\eta$ and use a relevant δ_N for the $\bar{p}p$ scattering.

For very small q^2 ($q^2 \le 0.2$ GeV^2), the real and imaginary parts of $f_{N,c}^{\rm Corr}$ can be fitted using the following parametrization. For example, the real part of $f_{N,c}^{\rm Corr}$ is

TABLE I. The parameters in the fit in Eq. (16) to the real and imaginary parts of $f_{N,c}^{\mathrm{Corr}}$.

Parameters	a_0	b_0	a_1	b_1	a_2	b_2	a_3	b_3
pp Real part	0.00553	0.01856	0.01998	−0.07130	−0.56648	0.33070	1.5591	−0.54019
pp Imaginary part	0.00497	−0.00353	−0.021147	0.01442	0.12403	−0.07913	1.5591	0.15702
$\bar{p}p$ Real part	−0.00743	−0.01842	−0.01278	0.07083	0.53333	−0.32971	−1.5049	0.54266
$\bar{p}p$ Imaginary part	−0.00471	0.00268	0.02029	−0.01061	−0.12343	0.05257	0.24633	−0.08269

$$\Re f_{N,c}^{\mathrm{Corr}}(s,t) = -(a_0 + b_0 \ln p)\ln t + (a_1 + b_1 \ln p) + (a_2 + b_2 \ln p)t + (a_3 + b_3 \ln p)t^2, \quad (16)$$

where a_i and b_i, $(i = 0,\ 1,\ 2,\ 3)$, are the parameters whose units are $\sqrt{\mathrm{mb}}/\mathrm{GeV}$, $\sqrt{\mathrm{mb}}/\mathrm{GeV}$, $\sqrt{\mathrm{mb}}/\mathrm{GeV}^3$, and $\sqrt{\mathrm{mb}}/\mathrm{GeV}^5$, for $i = 0$, 1, 2, and 3, respectively. The imaginary part will be fitted using the same form with a different set of the parameters. The parameters in the fit are given in Table I.

We note that the results for the corrections are essentially model independent: any model that fits the data at small q^2, respects unitarity, and has the correct analytic phase structure will give the same correction to the accuracy needed.

We can now write the full amplitude in a form,

$$f(s,q^2) = f_1(s,q^2) + f_N(s,q^2), \quad (17)$$

where the purely nuclear amplitude appears explicitly, with the Coulomb amplitude and the mixed Coulomb-nuclear corrections in f_1,

$$f_1(s,q^2) = f_c(s,q^2) + f_c^{FF}(s,q^2) + f_{N,c}^{\mathrm{Corr}}(s,q^2). \quad (18)$$

With our normalization, the differential elastic scattering amplitude is

$$\frac{d\sigma}{dq^2}(s,q^2) = \pi |f(s,q^2)|^2 \quad (19)$$

$$= \pi\left(|f_1|^2 + \frac{2|f_1||f_N|}{(1+\rho^2)^{1/2}}(\sin\Phi_1 + \rho\cos\Phi_1) + |f_N|^2\right), \quad (20)$$

where Φ_1 is the phase of $f_1(s,q^2)$ and $\rho(s,q^2) = \Re f_N(s,q^2)/\Im f_N(s,q^2)$. As mentioned in [1], at high energies, $\Re f_N$ has a zero at small q^2, $\Re f_N(s,q_R^2) = 0$, and, similarly, $\Im f_N(s,q_I^2) = 0$ at the first diffraction dip in $d\sigma/dq^2$ at $q_I^2 > q_R^2$. The zero in $\Re f_N$ is the expected Martin zero [23]. The possible effects of this zero were discussed in Kohara *et al.* [24] and included in the analysis of Pacetti *et al.* [25], and were included in our recent work [1] as well. We showed in fact that a reasonable approximate expression for the eikonal $\rho(s,q^2)$ from $q^2 = 0$ through the region of the Martin zero was $\rho(s,q^2) \approx \rho(s)\frac{1-q^2/q_R^2}{1-q^2/q_I^2}$ where q_R and q_I are the locations of the zeros in $\Re f_N$ and $\Im f_N$, respectively.

III. APPLICATIONS

A. Fits to the differential cross sections

As an application of the above-mentioned results, we consider the model in Eq. (2), which has been used frequently in the analysis of experimental data, *e.g.*, the TOTEM data at 8 and 13 TeV and the ATLAS data at 13 TeV; see Refs. [16,17,20] and earlier references therein. In this model, the phase of the nuclear amplitude is taken as a constant independent of q^2. It is determined simply by the ratio ρ of the real to the imaginary parts of the nuclear amplitude in the forward direction, corresponding to a phase $\Phi_N(s,q^2)$ and $f_N(s,q^2) = e^{i\Phi_N}|f_N(s,q^2)|$.

From Eq. (2), taking the square root and introducing the phase of the nuclear amplitude $\Phi_N = \frac{\pi}{2} - \arctan\rho(s,q^2)$, we have [26]

$$\sqrt{\pi} f_N(s,q^2) \approx \sqrt{A} e^{i\Phi_N} e^{-\frac{1}{2}(Bq^2 - Cq^4 + Dq^6 - \cdots)}. \quad (21)$$

Here, we use the form of the hadronic cross section in Eq. (2), with C and D taken from our eikonal results [27] and A, B, and ρ used as the fitting parameters, to reanalyze the experimental data at 53 GeV, 62.3 GeV, 8 TeV, and 13 TeV. We have included the Coulomb scattering corrections and the Coulomb-hadronic interference terms in these fits. Our eikonal results give $C = 9.770\ \mathrm{GeV}^{-4}$, $D = 18.83\ \mathrm{GeV}^{-6}$ at 53 GeV, $C = 10.29\ \mathrm{GeV}^{-4}$, $D = 19.98\ \mathrm{GeV}^{-6}$ at 62.3 GeV, $C = 9.176\ \mathrm{GeV}^{-4}$, $D = 26.53\ \mathrm{GeV}^{-6}$ at 8 TeV, and $C = 7.896\ \mathrm{GeV}^{-4}$, $D = 28.50\ \mathrm{GeV}^{-6}$ at 13 TeV, respectively. In Fig. 1, we show our calculated values of B, C, and D as functions of the center-of-mass energy $W = \sqrt{s}$ for the local momentum transfer $q_0^2 = 10^{-6}\ \mathrm{GeV}^2$ for pp (solid blue curves) and $\bar{p}p$ (dashed red curves). The curves are cut off at 50 GeV at the lower end. The behavior at the lower energies is largely the result of the importance of the Regge-like terms in the eikonal function at lower energies. For each parameter B, C, and D, respectively, the curves for pp and $\bar{p}p$ are identical at high energies as expected.

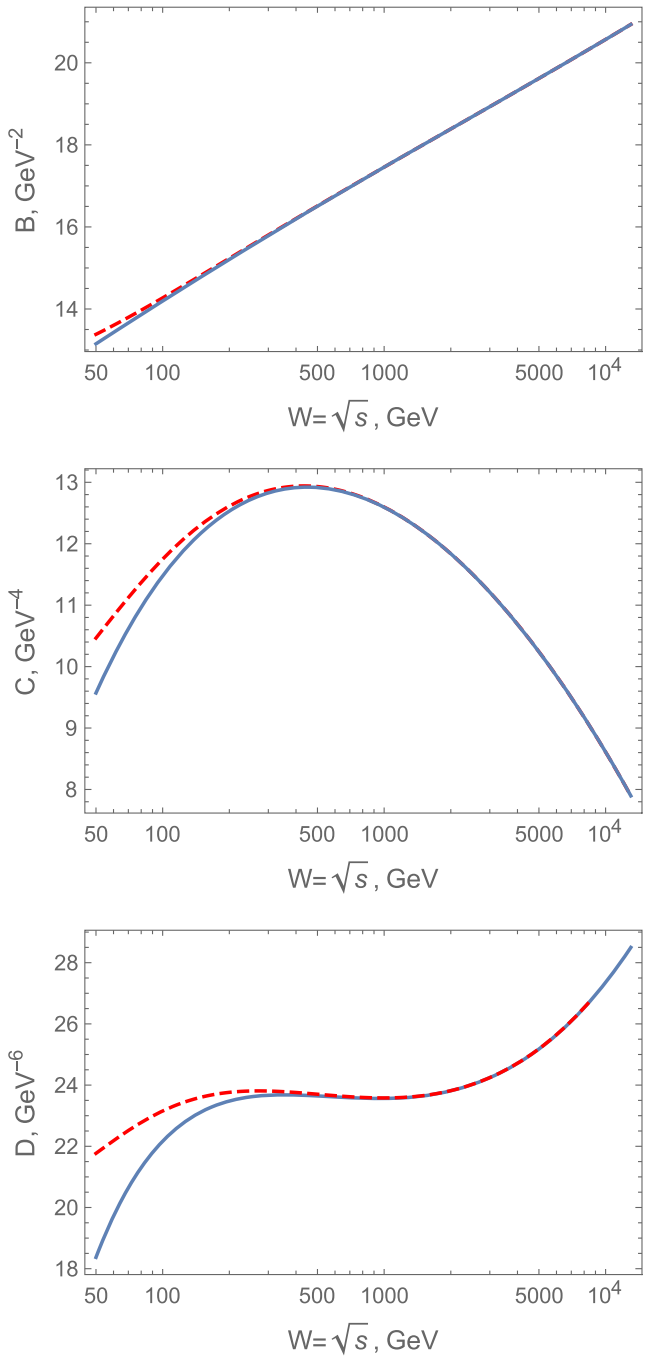

FIG. 1. Plot of the values of B, C, and D, calculated using our eikonal approach, versus $W = \sqrt{s}$ for the local momentum transfer $q_0^2 = 10^{-6}$ GeV^2 for pp (solid blue curves) and $\bar{p}p$ (dashed red curves). The behavior at the lower energies is largely the result of the importance of the Regge-like terms in the eikonal function at lower energies. For each parameter B, C, and D, respectively, the curves for pp and $\bar{p}p$ are identical at high energies as expected.

We have analyzed the fits using data up to a maximum value $q^2_{\max}$. We emphasize that our analyses are based on straightforward least squares fits to the rather precise data at those energies using only the quoted statistical errors. In Table II, we summarize the results of our fits to the ISR data at 53 GeV and 62.3 GeV for $q^2_{\max} = 0.1$ GeV^2 and fits to TOTEM data at 8 TeV and 13 TeV for $q^2_{\max} = 0.07$ GeV^2, 0.10 GeV^2, and 0.15 GeV^2. For each of the fits presented there, the total cross-section was derived via the optical theorem,

$$\sigma^2_{\text{tot}} = \frac{16\pi A}{1+\rho^2}. \tag{22}$$

For the TOTEM data at 8 TeV and 13 TeV, the fits for case 1) ($q^2_{\max} = 0.07$) and case 2) ($q^2_{\max} = 0.10$) are all excellent with χ^2/d.o.f. less than 1. The results from the fits are consistent with those found by the TOTEM Collaboration. As an illustration, we show the fits to $d\sigma/dq^2$ for the TOTEM data at 8 TeV and 13 TeV in Fig. 2 over the interval $q^2 \leq 0.10$ GeV^2 in conventional logarithmic plots.

We also use Eq. (2) to study the case of $C = D = 0$ (i.e., no curvature corrections) for the TOTEM data at 8 TeV and 13 TeV. We find that omitting D and C does not change ρ much because the only sensitivity to ρ is at very small q^2 where C and D terms are very small. However, the cross section fits over the region shown in Fig. 2 would be much worse if they are omitted.

Doing some fits with our variable $\rho(s, q^2)$ in the earlier paper [1] for $q^2 < 0.1$ GeV^2, we have found that the fit results and the fitting parameters do not change noticeably relative to the present results. The possible influence on ρ of the Martin zero in $\Re f_N$ is one of the main points in Kohara *et al.* [24] and Pacetti *et al.* [25]. In particular, Pacetti *et al.* get a significant effect not by using their q^2—dependent expression and fitting with that, but simply note that using an average of the variable result over the fitting range leads to a smaller fitted ρ. Like us, others have found no significant change when $\rho(s, q^2)$ is allowed to vary. This is because the sensitivity to the Coulomb-nuclear interference in the fitting is only at very small q^2.

B. The differential cross section $d\sigma/dq^2$ in the dip region

In order to see what differences one would expect in the eikonal model with Coulomb corrections, we look at the region near the observed dip in the differential cross section $d\sigma/dq^2$ for pp and $\bar{p}p$ elastic scattering. It is known that the cross sections in the dip region are very sensitive to small effects, and the data, especially the pp and $\bar{p}p$ differences which are affected by different normalization uncertainties on the two cross sections, are uncertain there. Thus, one cannot really specify an experimental difference at a point.

In Fig. 3, we plot the differential cross sections in the dip region for pp and $\bar{p}p$ at $W = 53$ GeV (top panel) and

TABLE II. The results of our fits to the ISR data at 53 GeV and 62.3 GeV [13–15] and to the TOTEM data at 8 TeV and 13 TeV [16,17]. The Coulomb and Coulomb-hadronic interference contributions to the scattering were included in the fit. A, B, and ρ are the corresponding parameters in fits, which included the curvature parameters C and D, with $(d\sigma/dq^2)_N \approx A\exp(-Bq^2 + Cq^4 - Dq^6)$. The parameters C and D were calculated using the comprehensive eikonal fit to the high energy pp and $\bar{p}p$ data in [18].

(GeV^2)	W (GeV)	d.o.f	χ^2/d.o.f.	A ($\mathrm{mb/GeV}^2$)	B (GeV^{-2})	ρ	σ_{tot} (mb)
1) $q^2_{\mathrm{max}} = 0.07$	13000	76	0.869	647.2 ± 0.7	21.23 ± 0.03	0.095 ± 0.004	112.0 ± 0.1
	8000	15	0.775	552.3 ± 2.9	20.68 ± 0.12	0.105 ± 0.020	103.4 ± 0.3
2) $q^2_{\mathrm{max}} = 0.10$	13000	93	0.956	645.8 ± 0.6	21.16 ± 0.02	0.091 ± 0.004	112.0 ± 0.1
	8000	18	0.710	551.5 ± 2.5	20.63 ± 0.08	0.102 ± 0.019	103.4 ± 0.3
	62.3	19	1.448	97.56 ± 0.72	13.40 ± 0.18	0.071 ± 0.018	43.59 ± 0.17
	53	18	2.048	92.98 ± 0.21	13.40 ± 0.07	0.082 ± 0.002	42.52 ± 0.05
3) $q^2_{\mathrm{max}} = 0.15$	13000	116	1.290	644.1 ± 0.5	21.09 ± 0.01	0.085 ± 0.004	111.9 ± 0.1
	8000	23	1.330	547.3 ± 2.1	20.43 ± 0.06	0.086 ± 0.018	103.1 ± 0.3

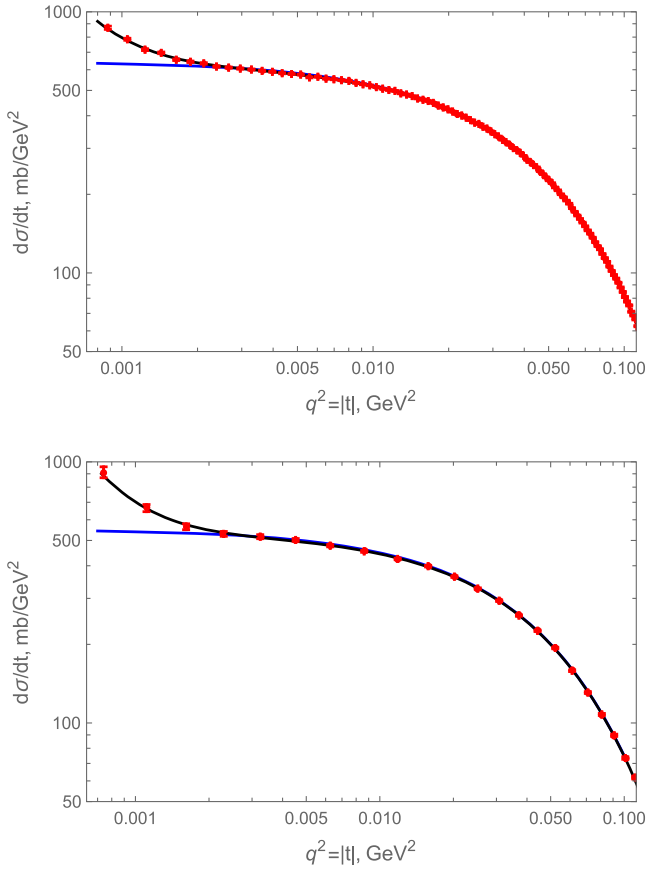

FIG. 2. Fits to the differential pp elastic scattering cross sections $d\sigma/dq^2$ for the TOTEM data at 8 TeV (bottom panel) and 13 TeV (top panel) over the interval $q^2 \leq 0.10\ \mathrm{GeV}^2$. The values of the curvature terms C and D in the series expansion of the hadronic contribution to $\ln(d\sigma/dq^2)$ were taken from the overall eikonal fit to the high-energy pp and $\bar{p}p$ data in [18]. $d\sigma/dq^2$ from the fit and the purely nuclear result of the fit are given by the black and blue curves, respectively. Data with their statistical errors are red.

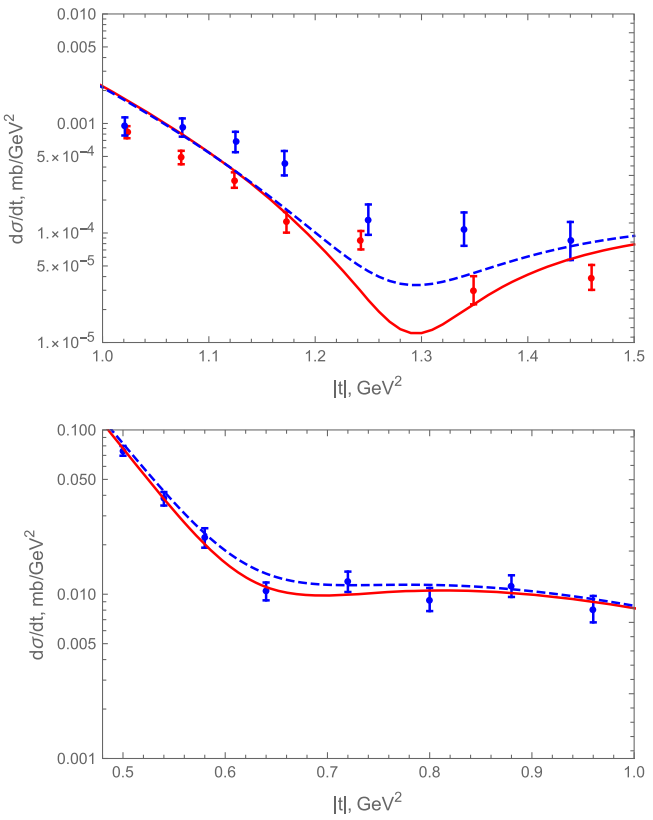

FIG. 3. Differential cross sections $d\sigma/dq^2$ in the dip region for pp and $\bar{p}p$ at $W = 53$ GeV (top panel) and 1.96 TeV (bottom panel). The red, solid curve and the blue, dashed curve are the differential cross sections $d\sigma/dq^2$ for pp and $\bar{p}p$ from our eikonal model with Coulomb corrections. Note that data for pp (red) and $\bar{p}p$ (blue) with their statistical errors at $W = 53$ GeV [13,14] are shown in the top panel and that only data for $\bar{p}p$ (blue) with their statistical errors at $W = 1.96$ TeV [29] are available in the bottom panel.

1.96 TeV (bottom panel). In the figure, the theoretical differential cross sections $d\sigma/dq^2$ from our eikonal model with Coulomb corrections for pp and $\bar{p}p$ are the red, solid curve and the blue, dashed curve, respectively. Note that data for pp (red) and $\bar{p}p$ (blue) with their statistical errors at $W = 53$ GeV [13,14] are shown in the top panel and that only data for $\bar{p}p$ (blue) with their statistical errors at $W = 1.96$ TeV [29] are available in the bottom panel.

We see that, at $W = 53$ GeV, our theoretical curves for $\bar{p}p$ and pp show a dip from the first diffraction zero in the dominant imaginary part of the nuclear scattering amplitude. This is predicted to be at $|t| = 1.295$ GeV^2, which is close to the observed minimum [13]. However, the ratio $d\sigma^{\bar{p}p}/d\sigma^{pp} = 2.76$ evaluated at the dip location $|t| = 1.295$ GeV^2 is smaller than the experimental value 4.5 ± 1.7 at $|t| = 1.333$ GeV^2 quoted in [14]. While some very small adjustment of the nuclear amplitude would be needed to obtain a more precise fit to the data, that is unlikely to change the conclusion that Coulomb-nuclear interference effects are significant in this region where the amplitude becomes predominantly real, and that those effects lead to a very significant difference between the pp and $\bar{p}p$ cross sections near the dip.

At $W = 1.96$ TeV, both our theoretical curves for pp and $\bar{p}p$ seem to agree with the D0 data for $\bar{p}p$ [29] but the curves do not show clearly a dip location. The predicted location of the zero in the imaginary part of the pp amplitude is $|t| = 0.638$ GeV^2. There are currently no pp data at 1.96 TeV, and the only information on cross section differences comes from the D0/TOTEM work using extrapolated pp cross sections [21]. We find that the Coulomb effects in the dip region at 1.96 TeV are still significant on the scale of the projected differences given in [21], Fig. 4, and should be included in analyzing those differences.

We conclude that Coulomb effects are significant in the dip region at 53 GeV and 1.96 TeV, and must be taken into account in searches for odderon effects through cross section differences in that region and energy range. The interference effects in the dip region are smaller at higher energies but are still significant. For example, the difference at 7 TeV is about 20% of the mean cross section at the dip at $|t| = 0.478$ GeV^2, about the same as the statistical uncertainty in the measured $\bar{p}p$ cross section.

IV. CONCLUSIONS

Using the simple eikonal approach for Coulomb-nuclear interference and form-factor effects and taking into account the curvature corrections in proton-proton scattering, we have fitted the parameters B, ρ, and σ_{tot} at $\sqrt{s} = 53$ GeV, 62.3 GeV, 8 TeV, and 13 TeV. We find that the results of the basic parameters calculated using our simple eikonal approach agree well with the results obtained using other methods.

We have also investigated the differential cross sections in the dip region for pp and $\bar{p}p$ elastic scattering at $W = 53$ GeV and 1.96 TeV and find that Coulomb effects are significant in the dip region at 53 GeV and 1.96 TeV, and must be taken into account in searches for odderon effects through cross section differences in that energy region.

ACKNOWLEDGMENTS

The author would like to thank Professor Loyal Durand for useful comments and invaluable support.

[1] L. Durand and P. Ha, Coulomb-nuclear interference effects in proton-proton scattering: A simple new eikonal approach, Phys. Rev. D **102**, 036025 (2020).
[2] H. A. Bethe, Scattering and polarization of protons by nuclei, Ann. Phys. (N.Y.) **3**, 190 (1958).
[3] G. B. West and D. R. Yennie, Coulomb interference in high-energy scattering, Phys. Rev. **172**, 1413 (1968).
[4] R. Cahn, Coulombic-hadronic interference in an eikonal model, Z. Phys. C **15**, 253 (1982).
[5] M. M. Islam, Bethe's formula for Coulomb-nuclear interference, Phys. Rev. **162**, 1426 (1964).
[6] V. Kundrát and M. Lokajíček, High-energy elastic scattering amplitude of unpolarized and charged hadrons, Z. Phys. C **63**, 619 (1994).
[7] N. H. Buttimore, E. Gotsman, and E. Leader, Spin-dependent phenomena induced by electromagnetic-hadronic interference at high energies, Phys. Rev. D **18**, 694 (1978).
[8] B. Z. Kopeliovich and A. V. Tarasov, The Coulomb phase revisited, Phys. Lett. B **497**, 44 (2001).
[9] M. M. Block, Hadronic forward scattering: Predictions for the Large Hadron Collider and cosmic rays, Phys. Rep. **436**, 71 (2006).
[10] M. M. Block and R. N. Cahn, High-energy $p\bar{p}$ and pp forward elastic scattering and total cross sections, Rev. Mod. Phys. **57**, 563 (1985).
[11] G. Pancheri and Y. Srivastava, Introduction to the physics of the total cross section at LHC, Eur. Phys. J. C **77**, 150 (2017).
[12] M. M. Block, L. Durand, P. Ha, and F. Halzen, Eikonal fit to pp and $\bar{p}p$ scattering and the edge in the scattering amplitude, Phys. Rev. D **92**, 014030 (2015).
[13] E. Nagy *et al.*, Measurement of elastic proton-proton scattering at large momentum transfer at the CERN intersecting storage rings, Nucl. Phys. **B150**, 221 (1979).

[14] A. Breakstone *et al.*, Measurement of $\bar{p}p$ and pp Elastic Scattering in the Dip Region at $\sqrt{s} = 53$ GeV, Phys. Rev. Lett. **54**, 2180 (1985).

[15] N. Amos *et al.*, Measurement of small angle antiproton-proton and proton proton elastic scattering at the CERN intersecting storage rings, Nucl. Phys. **B262**, 689 (1985).

[16] G. Antchev *et al.* (TOTEM Collaboration), Measurement of elastic pp scattering at $\sqrt{s} = 8$ TeV in the Coulomb-nuclear interference region—determination of the ρ parameter and total cross section, Eur. Phys. J. C **76**, 661 (2016).

[17] G. Antchev *et al.* (TOTEM Collaboration), First determination of the ρ parameter at $\sqrt{s} = 13$ TeV, Eur. Phys. J. C **79**, 785 (2019).

[18] L. Durand and P. Ha, Eikonal and asymptotic fits to high-energy data for σ, ρ, and B: An update with curvature corrections, Phys. Rev. D **99**, 014009 (2019).

[19] M. M. Block, L. Durand, P. Ha, and F. Halzen, Slope, curvature, and higher parameters in pp and $\bar{p}p$ scattering, and the extrapolation of measurements of $d\sigma(s,t)/dt$ to $t = 0$, Phys. Rev. D **93**, 114009 (2016).

[20] H. Stenzel (ATLAS Collaboration), Determination of the total cross section and ρ-parameter from elastic scattering in pp collisions at $\sqrt{s} = 13$ TeV with the ATLAS detector, Proc. Sci. ICHEP2022 (**2022**) 803 [arXiv:2209.11487].

[21] V. Abazov *et al.* (The D0 and TOTEM Collaborations), Odderon Exchange from Elastic Scattering Differences between $\bar{p}p$ and pp data at 1.96 TeV and from pp Forward Scattering Measurements, Phys. Rev. Lett. **127**, 062003 (2021).

[22] Magnetic-moment scattering does not contribute to the spin-independent part of the scattering amplitude. Its contribution to the spin-dependent amplitude is also suppressed by an angular factor proportional to $\sqrt{q^2}$ at small q^2. The factor $1/q^2$ from the photon propagator therefore partially cancels and the amplitude is suppressed relative to the charge-scattering term for $q^2 \to 0$. The magnetic form factors $F_M^2(q^2)$ further suppress the scattering at large q. As a result, the magnetic terms do not contribute significantly to the scattering in the region of interest here. See a detail discussion in [1].

[23] A. Martin, A theorem on the real part of the high-energy scattering amplitude near the forward direction, Phys. Lett. B **404**, 137 (1997).

[24] A. K. Kohara, E. Ferreira, T. Kodama, and M. Rangel, Elastic amplitudes studied with the LHC measurements at 7 and 8 TeV, Eur. Phys. J. C **77**, 877 (2017).

[25] S. Pacetti, Y. Srivastava, and G. Pancheri, Analysis and implications of precision near-forward TOTEM data, Phys. Rev. D **99**, 034014 (2019).

[26] We have considered the variation of ρ in the earlier paper [1] taking into account the nearby diffraction zero in the real part of the amplitude, but that this q^2 dependence of ρ does not significantly affect our results because the interference effects which determine ρ are limited to a very small range of q^2 near $q^2 = 0$.

[27] The expansion in Eq. (2) and its range of validity were investigated in detail in [19], where exact expressions were given for the parameters B, C, and D in the eikonal approach. As noted there, the predicted values of those parameters were consistent with the results obtained by TOTEM Collaboration in their fits to their TeV data [28].

[28] G. Antchev *et al.* (TOTEM Collaboration), Evidence for non-exponential elastic proton-proton differential cross section at low $|t|$ and $\sqrt{s} = 8$ TeV, Nucl. Phys. **B899**, 527 (2015).

[29] V. Abazov *et al.* (D0 Collaboration), Measurement of the differential cross section $d\sigma/dt$ in elastic $p\bar{p}$ scattering at $\sqrt{s} = 1.96$ TeV, Phys. Rev. D **86**, 012009 (2012).